# Molecular Dynamics Simulation on Collision Frictional Properties of a Molybdenum Disulfide ($MoS_2$) Film in Microgravity Environment

Ruiting Tong[1,*] · Bin Han[2] · Xiao Zhang[1] ·Tao Zhang[3] · Quanren Zeng[4] · Geng Liu[1]

[1] Shaanxi Engineering Laboratory for Transmissions and Controls, Northwestern Polytechnical University, Xi'an 710072, China

[2] Jiangsu Automation Research Institute, Lianyungang 222006, China

[3] CALT, China Academy of Launch Vehicle Technology, Beijing 100076, China

[4] Department of Design, Manufacturing and Engineering Management, University of Strathclyde, Glasgow, G1 1XQ, UK

*Corresponding author. Email: tongruiting@nwpu.edu.cn; Tel: +86-13892823204

**Abstract**

In this paper, a collision friction model for a double-layer $MoS_2$ film is proposed considering the microgravity induced collision in space environment. A modified REBO (Reactive Empirical Bond Order) potential is used to describe interactions among the atoms in the $MoS_2$ film. The collision friction process of the $MoS_2$ film is simulated by vibrations in the *y* and *z* directions, and the dependence of average friction force is analyzed. The influence of a single vibration in the *y* direction on the friction forces can be ignored, while the vibration in the *z* direction shows great influence. The effects of vibration frequency and amplitude on frictional behaviors of the $MoS_2$ film are investigated. The average friction forces during the collision friction process correlate with the frequency of the vibration in the *z* direction, and the relationship shows four stages. As the frequency increases, average friction forces show low values in the first stage, and they are increased as the frequency in the second stage. In the third stage, the average friction forces are decreased, and they come to a stable level in the fourth stage. Increasing the vibration amplitude at different frequencies leads to an increase in average friction force, due to that the increased amplitude results in a high indentation depth. The puckering phenomenon occurs at a specific frequency, which is a reason that the average friction force is increased during this collision friction process.

**Keywords**: Molybdenum disulfide · Collision effects · Frictional properties · Molecular dynamics · Microgravity environment

# 1. Introduction

Due to the non-zero bandgap of material nature, molybdenum disulfide ($MoS_2$) is considered as a promising alternative to graphene (Wang et al. 2018). The interactions between S and Mo atoms within a $MoS_2$ layer are dominated by strong covalent bonds, while the interactions between adjacent $MoS_2$ layers are dominated by Van der Waals forces (Park et al. 2020). Therefore, $MoS_2$ shows excellent frictional properties and has been widely used as a solid lubricant (Stewar and Spearot 2013; Irving et al. 2017). Especially, $MoS_2$ is widely used in space environment because of its stable frictional properties in vacuum environment (Hou et al. 2018; Zeng et al. 2019).

There are many studies on friction mechanisms and properties of $MoS_2$. Spalvins (1969) obtained $MoS_2$ films by physical sputtering and investigated its lubricating properties in vacuum environment. The friction experiments showed low coefficients of friction and long endurance lives for $MoS_2$ films. A further work of Spalvins (1978) attributed the excellent lubricating properties of sputtered $MoS_2$ films to their strong adherence to the substrate. The lubrication mechanism of $MoS_2$ was investigated by a scanning electron microscope in the work of Holinski and Gänsheimer (1972), and the excellent frictional properties were attributed to strong polarization of S atoms. Friction, wear and optical microscopy studies on $MoS_2$ films in moist air, dry air and dry argon environment were performed by Fusaro (1978). The results showed that friction forces in moist air were higher than those in dry air and dry argon due to the rapid transformation of $MoS_2$. The lubrication mechanism consisted of the formation of a thin, coalesced $MoS_2$ film on each sliding surface during the initial stages of sliding and subsequent continual plastic flow of this film between the sliding surfaces. The further work of Fusaro (1982) concluded that the lubrication mechanism was the plastic flow of $MoS_2$ thin films between the flat plateaus on the hemispherically tipped indenter and on the metallic substrate. For sputtered $MoS_2$ thin films, Fleischauer (1984) found that when the crystallites were arranged with their basal planes parallel to the substrate surface, the films showed better stability and longer endurance lives than those with randomly-oriented crystallites. A further work from Fleischauer and Bauer (1988) demonstrated that the lubricating properties of sputtered $MoS_2$ films were related to the crystallite size, and larger particles induced lower friction coefficients during the initial stage of friction. Pope and Panitz (1988) pointed out that a high working pressure could improve the formation of transfer films on the interface and reduce the period to form an equilibrium particle size of $MoS_2$. This hence led to the decrease of friction coefficients of $MoS_2$ coatings as Hertzian stress increased when testing in air. Furthermore, testing in ultrahigh vacuum showed reduced friction coefficients when compared with those tested in air. Singer et al. (1990) found that frictional properties were influenced by the applied load, and friction coefficients of the $MoS_2$ coating under elastic contact conditions decreased as the applied load increased. Colas et al. (2013) suggested that more degrees of freedom for $MoS_2$ coatings could offer lower friction and longer life, and they attributed the bad frictional behaviors of non-columnar amorphous coatings to the lack of degrees of freedom. Takahashi et al. (1991) used a high resolution transmission electron microscope (HRTEM) to study sliding contact properties of $MoS_2$. The stacking fault was observed by the HRTEM and it verified the transformation from h.c.p. to f.c.c. at an atomic scale.

Considering that micro/nano scale behaviors of $MoS_2$ will influence overall frictional performance, the micro/nano scale experiments or simulations are performed to investigate the correlation. Li et al. (2016) studied frictional characteristics of $MoS_2$ by experiments and simulations, and found that friction forces varied with lattice orientations. The studies of Li et al. (2017) provided an experimental evidence for superlubricity between $MoS_2$ atomic layers, and friction coefficients showed no dependence on the thickness of $MoS_2$ even it came to a single atomic layer. Cao et al. (2018) compared the lubricating performance of $MoS_2$ nanosheets and perfluorodecyltrichlorosilane self-assembled monolayers. The higher elastic modulus of $MoS_2$ nanosheets induced smaller contact areas and led to lower friction forces. Their further work investigated anisotropic frictional properties of $MoS_2$ with different thicknesses by a calibrated atomic force microscopy. The anisotropic nanofriction was attributed to the lattice orientation and puckering effect when the thickness was 4.18

nm, while the anisotropic nanofriction was mainly induced by the puckering effect for a thickness of 1.49 nm. As the thickness increases, nanofriction forces decreased, and the anisotropy ratio increased (Cao et al. 2019). Yang and Liu (2020) found that the substrate effect on frictional properties was decreased gradually when the thickness of a $MoS_2$ film was more than 6 layers. These phenomena (Cao et al. 2019; Yang and Liu 2020) are different from the conclusions of Li et al. (2017). Huang et al. (2019) studied the effects of the scanning velocity on nanotribological properties of $MoS_2$. They found that the friction force was increased as the scanning velocity increased and then became stable. Nanoscale friction experiments in the work of Serpini et al. (2019) indicated that ordered $MoS_2$ showed lower friction coefficient than disordered case, and simulation results agreed well with the experiments. The friction reduction of the ordered case was caused by partial layer incommensuration.

In addition to parameters of $MoS_2$ films and sliding parameters, the material or structure of the substrate also affect frictional characteristics. Quereda et al. (2014) experimentally studied friction forces of single-layer $MoS_2$ crystals deposited on $SiO_2$, mica and hexagonal boron nitride (h-BN), and the h-BN substrate remarkably reduced the roughness of the $MoS_2$ crystal and consequently reduced the friction force. Yang and Liu (2020) investigated frictional properties of $MoS_2$ films deposited on different substrates by atomic layer deposition (ALD). The $MoS_2$ film on $Al_2O_3$ showed the lowest friction, while the $MoS_2$ film on Si was the highest due to the effect of substrate on the specific self-limiting reaction in the ALD process. By AFM nanoindentation experiments, Huang et al. (2018a) found that $MoS_2$ nanosheets were more prone to be damaged when suspended on holes compared with that supported on the substrate under the same conditions. It could be attributed to the smaller deformation and better heat conduction when supported on the substrate. This conclusion could be used to explain the influence of the roughness in the work of Quereda et al. (2014). In another work of Huang et al. (2018b), the friction of the suspended $MoS_2$ was much higher than the case of supported $MoS_2$ due to the lower bending stiffness and more severe puckering effect at the AFM tip-$MoS_2$ contact interface, and increasing applied load led to great difference. Besides, the friction decreased as the layers increased for both cases because of the enhanced bending stiffness. Xing et al. (2020) combined laser-induced periodic surface structures and ALD $MoS_2$ nano coatings to improve frictional performance. The results showed that friction forces were reduced greatly, and the combination of conformal groove structures and the lubricating film got the lowest friction force due to the reduced contact area and adhesion.

Experimental studies have obtained many valuable results, and numerical simulations were also performed to investigate the friction mechanism of $MoS_2$. Onodera et al. (2009) found that the predominant interaction between two sulfur layers in different $MoS_2$ sheets was Coulombic repulsion, which directly affected lubricating properties. The $MoS_2$ sheets adsorbed on an iron substrate reduced friction further due to much higher Coulombic repulsive interactions. Their further work (Onodera et al. 2010) pointed out that lubricating properties of $MoS_2$ strongly depended on its interlayer contacts at atomic scale. Pang et al. (2018b) investigated atomic scale frictional properties of a single-layer $MoS_2$ film by molecular dynamics (MD) simulation, and they found that increasing tip radius could increase the friction force, while the friction force decreased as the tip-substrate distance increased. By using MD simulation, Claerbout et al. (2019) found that the sliding direction showed great effects on frictional characteristics of commensurate $MoS_2$, and the incommensurability was not a necessary condition to obtain a superlubric behavior of $MoS_2$. Shi et al. (2019) performed reactive force-field MD simulation on the friction mechanism of $MoS_2$, and the interaction between S atoms at the interface was a main factor that influenced the friction.

From experimental and theoretical studies, atomic scale interactions among the atoms of $MoS_2$ play the key role in frictional behaviors. Considering that $MoS_2$ is widely used as a lubricant in space environment, the interatomic force is dominant in vacuum environment of outer space. In addition to vacuum environment, the microgravity-induced irregular collision also influenced frictional behaviors (Tong and Liu 2019, 2020a, 2020b). At meantime, the collision-induced high indentation depth may cause severe puckering effects that further affect the frictional performance of a $MoS_2$ film. The collision effects in microgravity environment were investigated with the simulation on frictional characteristics of Ag film (Tong et al. 2019b) or Au film (Tong et al. 2019a), and some of the collision energy could be passed to the substrate and caused dislocations. If a $MoS_2$ film is combined with ductile metal materials (e.g. Au), the frictional behaviors may be improved due to the energy transformation. Stoyanov et al. (2012) found that the wear resistance of Au/$MoS_2$ bilayer coatings could be improved in ground environment. Gao et al. (2020) exposed $MoS_2$-Au/Au multilayer films in low earth orbit space environment, and the exposed film showed good frictional properties after a relatively high initial friction coefficient when tested on the earth. In microgravity environment, when a mechanical component is disturbed, the component will vibrate randomly and hence cause collision friction. The collision energy will be transferred from a contact body to the other one, which could induce deformation or dislocation. When combining the $MoS_2$ film and Au, the collision energy can be transferred to the Au due to its low hardness, which will produce a synergistic effects to friction reduction. Up to now, the collision frictional performances of $MoS_2$ films on Au are rarely reported.

In this paper, a double-layer $MoS_2$ film is introduced to an Au surface, and a modified REBO potential is used to describe interactions among the atoms in the $MoS_2$ film. The microgravity environment induced collision effects are simulated by applying vibrations on the slider in two directions and a passive vibration on the substrate in one direction (Tong et al. 2019a). The collision friction process of the $MoS_2$ film is analyzed, and the effects of vibration frequency and amplitude on frictional properties of the $MoS_2$ film are investigated.

## 2. Modelling and method

Figure 1 shows a collision friction model including a rigid cylindrical slider and an elastic substrate. The substrate consists of a double-layer $MoS_2$ film and the underneath FCC Au. For the double-layer $MoS_2$ film, its stacking is AA1, which is the most stable structure (Ghobadi 2017). Two vibrations are applied on the slider in the *y* and *z* directions to simulate random vibrations in microgravity environment. Considering the vibration between the substrate and its connecting component, the bottom of the substrate is connected to a spring, and the stiffness of the spring is 800 N/m. The bottom 3 layers atoms are fixed, and 3 thermostatic layers are used above the fixed layers. The fixed layers can move in the *z* direction but cannot move in the *x* or *y* directions. The temperature of thermostatic layers is maintained at 300 K during the simulation. A NVE ensemble is applied in the Newtonian atoms. The material of the slider is Au. The radius of the cylindrical slider is 6.12 nm, and the length of the slider in the *y* direction is 6.53 nm. To improve computational efficiency, only the lower part of the slider is considered. The size of the substrate is 40.8 nm×6.53 nm×10.2 nm in the *x*, *y* and *z* directions, respectively, including 182368 atoms.

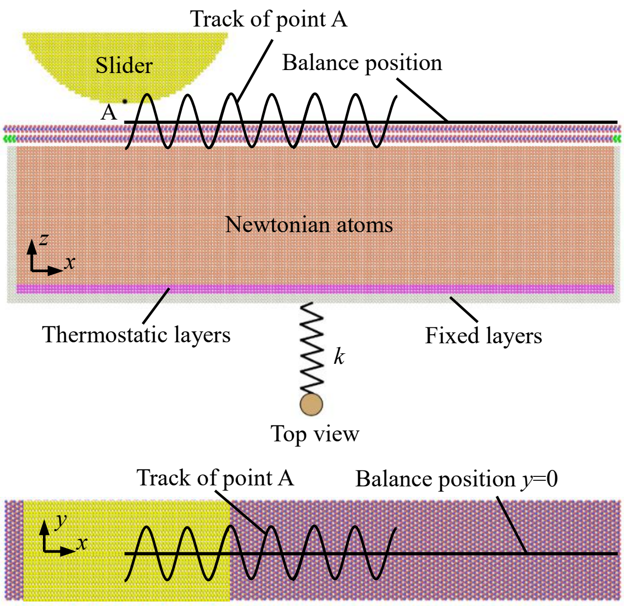


**Fig. 1** A collision friction model of $MoS_2$

For the double-layer $MoS_2$ film in Fig. 1, an illustrative structure is shown in Fig. 2. The thickness of a single-layer $MoS_2$ is 3.241 Å, and the spacing between two layers is 2.903 Å. The simulations are performed by using Large-scale Atomic/Molecular Massively Parallel Simulator (LAMMPS) (Plimpton 1995) and the results are visualized by OVITO (Stukowski 2010). Nicolini and Polcar (2016) compared the empirical potentials for sliding simulations of $MoS_2$, and they found that the REBO potential (Liang et al. 2009) was the most suitable one. To describe interactions of $MoS_2$, a modified REBO potential developed by Liang et al. (2009, 2012) is used in our model.

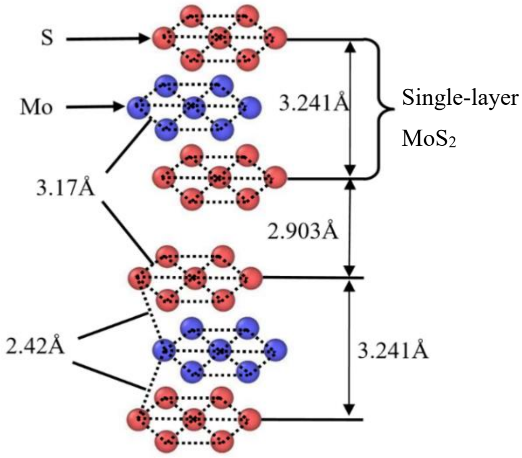


**Fig. 2** The structure of a double-layer $MoS_2$ film (Stewar and Spearot 2013)

The modified REBO potential is given as follows:

$$E = \frac{1}{2}\sum_{i \neq j} f_{ij}^{C}\left(r_{ij}\right)\left[V^{R}\left(r_{ij}\right) - b_{ij}V^{A}\left(r_{ij}\right)\right] \tag{1}$$

where $V^R$ is a repulsion interaction, $V^A$ is an attraction interaction, $b_{ij}$ is a bond-order function, and $f_{ij}^{C}$ is a cutoff function. An EAM potential is used to describe the interactions of substrate Au atoms and slider atoms. The interactions between Au and $MoS_2$ are described by L-J potential, and the L-J parameters of Au-S and Au-Mo are calculated by Lorentz-Berthelot (L-B) mixing rules (Delhommelle and Millie 2001; Wang et al. 2016). Distance parameters in the L-B mixing rules can be calculated as:

$$\sigma_{ij} = \frac{\left(\sigma_i + \sigma_j\right)}{2} \tag{2}$$

where $\sigma_i$ is the distance parameter of atom $i$, and $\sigma_j$ is the distance parameter of atom $j$. Energy parameters in the L-B mixing rules can be obtained as:

$$\varepsilon_{ij} = \sqrt{\varepsilon_i \varepsilon_j} \tag{3}$$

where $\varepsilon_i$ is the energy parameter of atom $i$, and $\varepsilon_j$ is the energy parameter of atom $j$.

The initial gap between the slider and the $MoS_2$ film is 15 Å, which is greater than the cutoff radius $r_c$ of L-J potential ($r_c$=10 Å). At the beginning, the slider moves down to contact with the $MoS_2$ film at a velocity of 50 m/s. Then a sliding velocity of 50 m/s is applied on the slider in the $x$ direction, and the time step is 0.004 ps. Two simple harmonic vibrations are applied on the slider in the *y* and *z* directions.

## 3. Results and discussion

$MoS_2$ is widely used in space environment as a solid lubricant due to its excellent frictional properties. In this paper, the average friction forces for the models with or without the double-layer $MoS_2$ film at different frequencies are compared in Fig. 3, and the amplitude of the vibrations in the *y* and *z* directions is 4 Å. From Fig. 3, the average friction forces during collision friction process are significantly reduced when the $MoS_2$ film is introduced. For the case of no $MoS_2$, the substrate is the FCC Au, and there are a great number of atoms accumulated in front of the slider during the collision sliding contact. The accumulated atoms results in large contact areas and high average friction forces. On the contrary, the contact areas between the slider and the $MoS_2$ film are small, which induce low average friction forces.

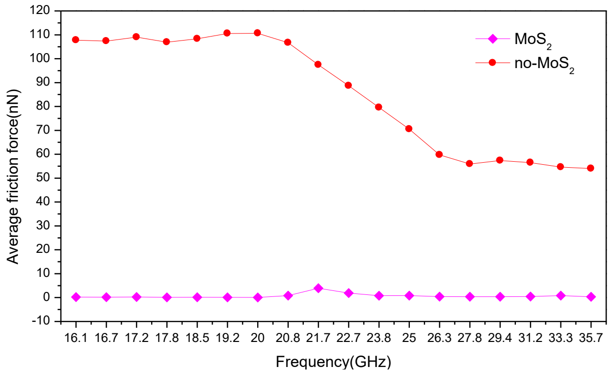


**Fig. 3** The comparison of average friction forces of the two models.

### 3.1 The effects of a single vibration on the collision frictional behaviors

In this work, there are vibrations on the slider in the *y* and *z* directions. From the parameters in Section 2, using the formula $f=(1/2\pi)(k/m)^{1/2}$ (where $k$ is the stiffness of the spring, and $m$ is the mass of the substrate), we can find that the natural frequency of the substrate is 18.5 GHz. To investigate the effects of a single vibration on collision frictional behaviors, four vibration frequencies of the slider are chosen, including 16.1 GHz, 18.5 GHz, 21.7 GHz and 50.0 GHz, which are only applied in the *y* direction.

Figure 4 shows friction forces of sliding contacts under a single vibration in the *y* direction, and the vibration function is $y=A\sin 2\pi ft$, where $A$=4 Å, is the amplitude, $f$ is the vibration frequency, and *t* is the sliding time. When considering the vibrations in the *y* direction, friction forces curves are similar to the case of no vibration, not only the values, but also the fluctuations.

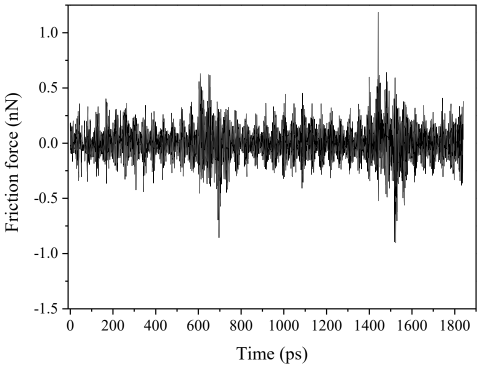


(a) no vibration

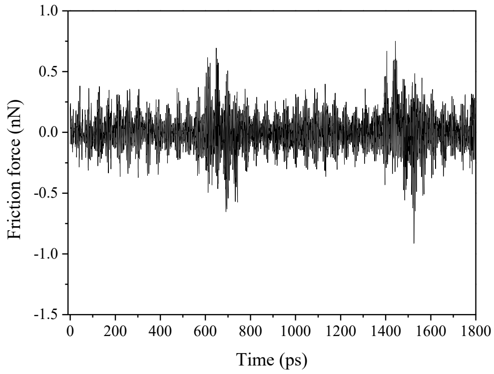


(b) *f*=16.1 GHz

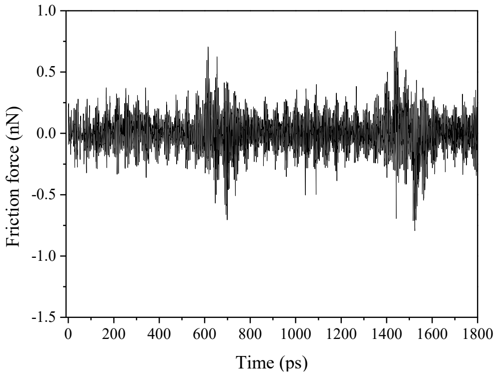


(c) *f*=18.5 GHz

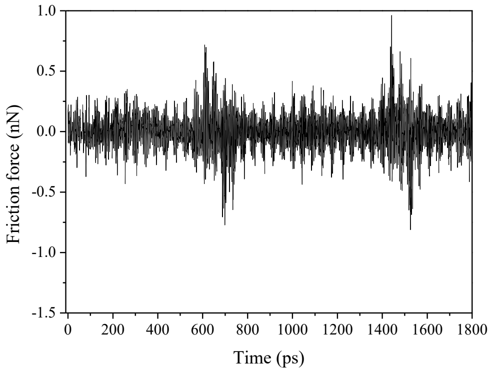


(d) *f*=21.7 GHz

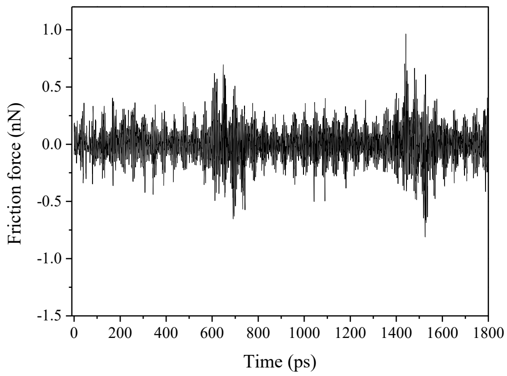


(e) *f*=50 GHz

**Fig. 4** Friction forces of sliding contacts under a single vibration in the *y* direction

Fig. 5 gives the average friction forces corresponding to the cases in Fig. 4. Compared with the average friction force of the no vibration case (0.378 nN), the average friction force of the case *f*=16.1 GHz (0.369 nN) shows the biggest difference among all the cases, and the difference is 2.38%. Then, we can conclude that there is little influence of the vibration in the *y* direction on frictional behaviors. At the nanoscale, the surface-to-volume ratio is very high, and the adhesive force plays a dominant role during the friction process. For the sliding contact considering the vibration in the *y* direction, there is little influence of the vibration on the contact area. As we know, the adhesive force is proportional to the contact area (Moore 1975), so the influence of the vibration in the *y* direction is slight.

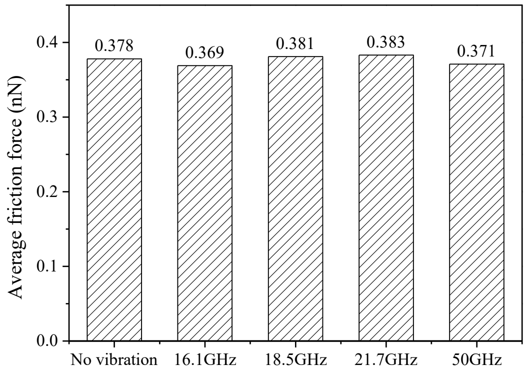


**Fig. 5** Average friction forces of sliding contacts under a single vibration in the *y* direction

To investigate the effect of a single vibration in the *z* direction on frictional behaviors, three vibration frequencies of the slider including 16.1 GHz, 18.5 GHz and 21.7 GHz are only applied in the *z* direction. The vibration function is $z=A\sin 2\pi ft$, where $A$=4 Å, is the amplitude, $f$ is the vibration frequency, and $t$ is the sliding time. Fig. 6 compares the friction forces of sliding contacts under a single vibration in the *z* direction with different frequencies. There is great difference in fluctuation amplitudes of the friction force curves. Considering the vibration in the *z* direction, the indentation depth of the slider will be influenced by the vibration process, and a large contact area is induced due to a high indentation depth, which produces a high adhesive force. Besides, according to the work of Tong et al. (2019c), in addition to the adhesive force in nanoscale sliding contacts, the ploughing component plays a role in a nanoscale sliding contact, and that is why the friction forces are vibrated so severely when the vibrations in the *z* direction are applied on the slider. Fig. 7 shows the average friction forces corresponding to the cases in Fig. 6. The highest value occurs at the frequency of 21.7 GHz, and it is about 10 times of the case with no vibration. Comparing Fig. 5 and Fig. 7, the average friction forces shows frequency dependence when considering the vibration in the *z* direction. Therefore, in the next sections, the vibration frequency in the *y* direction is kept at 50 GHz, and the effects of vibration frequency in the *z* direction on the friction forces are investigated.

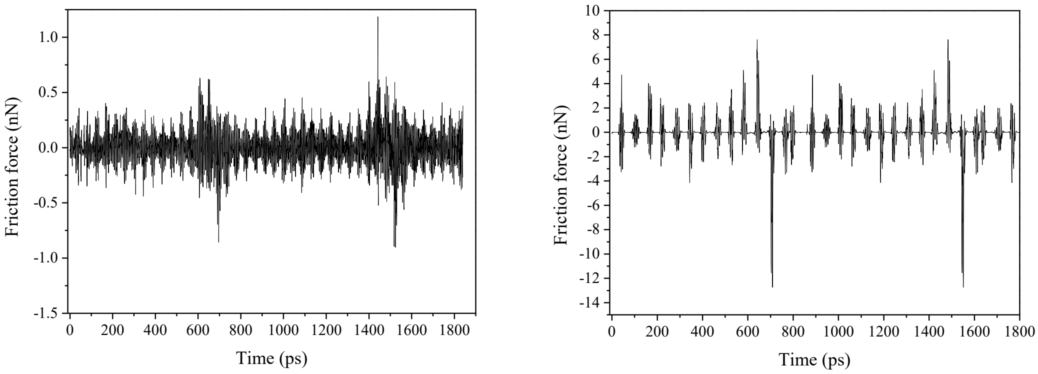


(a) no vibration (b) *f*=16.1 GHz

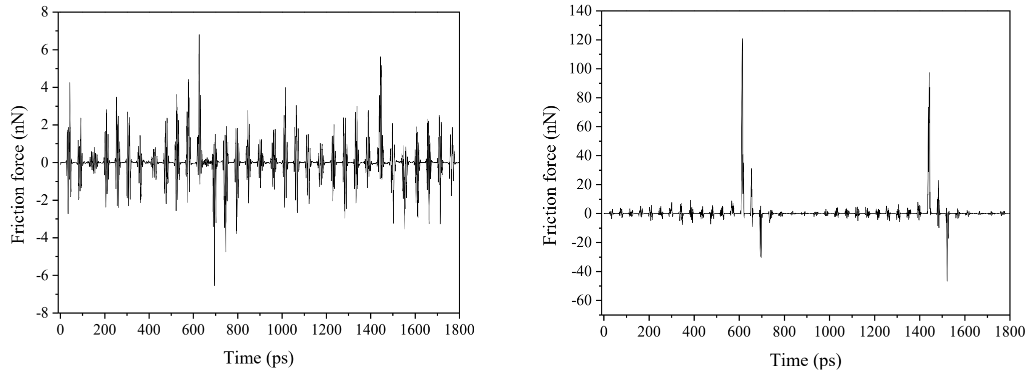


(c) *f*=18.5 GHz (d) *f*=21.7 GHz

**Fig. 6** Friction forces of sliding contacts under a single vibration in the *z* direction

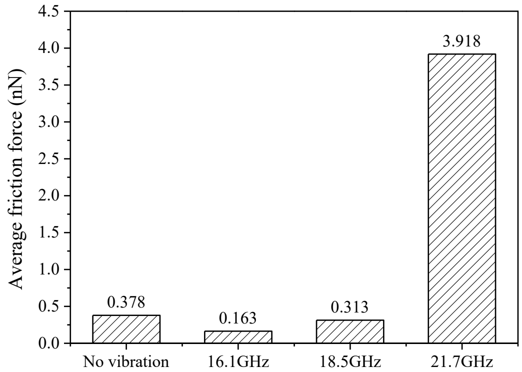


**Fig. 7** Average friction forces of sliding contacts under a single vibration in the *z* direction

### 3.2 The effects of frequency on collision friction process

In microgravity environment, friction forces of a soft metal showed frequency dependence when the collision effect was considered (Tong et al. 2019a). Fig. 8 shows average friction forces at different frequencies after a $MoS_2$ film is introduced. The variation of the average friction forces with frequency for the model with the $MoS_2$ film can be divided into 4 stages as shown in Fig. 8. In the first and fourth stages, the average friction forces show slight variation as the frequency increases. In the second stage, the average friction forces increase rapidly as the frequency increases. In the third stage, the average friction forces show a decrease trend.

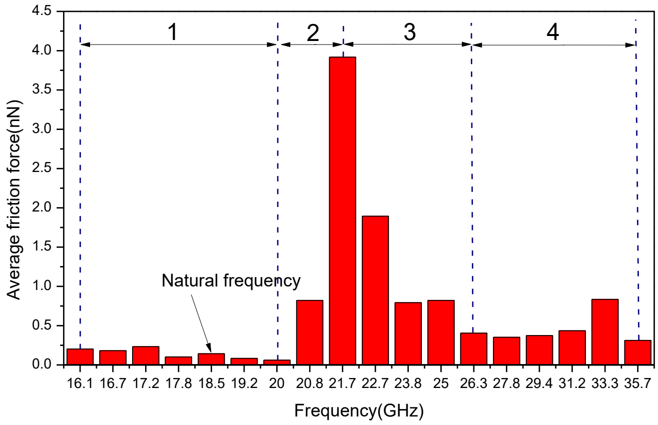


**Fig. 8** Average friction forces at different frequencies

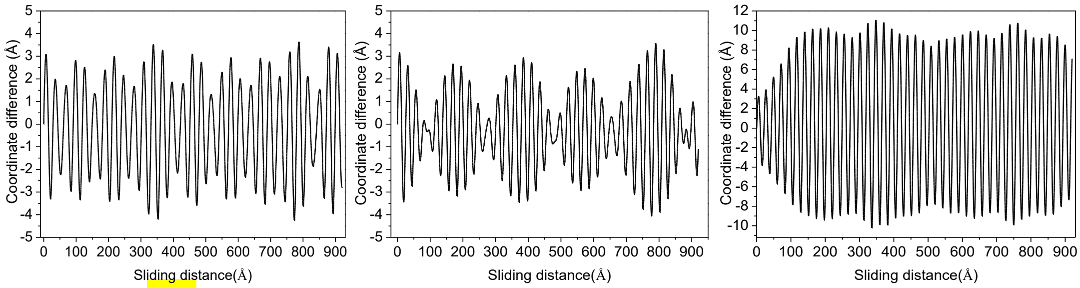


(a) 16.1 GHz (b) 18.5 GHz (c) 21.7 GHz

**Fig. 9** The coordinate difference between the slider and substrate at different frequencies

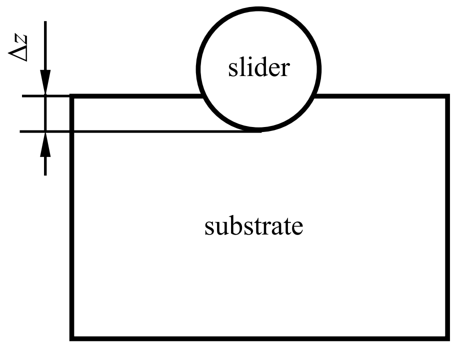


**Fig. 10** Schematic diagram of the coordinate difference between the slider and substrate

Figure 9 shows the coordinate difference between the slider and substrate at different frequencies. The coordinate difference $\Delta z$ is defined as the difference between the lowest atom of the slider and the topmost layer of the substrate in the $z$ direction, as shown in Fig. 10. The absolute value of the negative coordinate difference represents the indentation depth for each collision process. Combining Fig. 8 and Fig. 9, we find that the variation of average friction forces correlates with the variation of coordinate difference. The greater the coordinate difference between the slider and the substrate, the greater the average friction force. For Fig. 9(a) and (b), the frequencies stay in the first stage in Fig. 8, and the coordinate difference is kept around ±3-4 Å, that is to say, the maximum indentation depth is about 3-4 Å. The maximum indentation depth changes slightly with the frequency, so the average friction forces show little change with the frequency. From Fig. 9(c), the maximum indentation depth is about 10-11 Å for each collision process at the frequency of 21.7 GHz. For a cylindrical slider, a high indentation depth means a large contact area and a high adhesive force. Besides, the high indentation depth also induces a high ploughing component of a friction force (Moore 1975). These should be the reasons why the average friction force is the highest at the frequency of 21.7 GHz.

In the first stage, the vibration frequencies of the slider are close to the natural frequency of the substrate (18.5 GHz). Meanwhile, the collision between the slider and the substrate is not severe and the coordinate difference is maintained within a small range. Therefore, the average friction forces present low values and show small changes as the frequency increases. In the second stage, the collision between the slider and the substrate gradually becomes more severe as the frequency increases. The more severe the collision, the greater the indentation depth. A greater indentation depth induces a high adhesion component (due to a large contact area) and a high ploughing component of a friction force. Hence, the average friction forces are higher.

For the third stage, Fig. 11 and Fig. 12 show the velocities in the *z* direction of the slider and substrate at different frequencies. When the substrate velocity is greater than the slider velocity, collision occurs. When the substrate velocity is equal to the slider velocity, it is at the critical state of collision and separation, and the indentation depth is the maximum at this moment. When the substrate velocity is lower than the slider velocity, separation occurs. When the slider frequency is 21.7 GHz, the substrate is moving upwards and the slider is moving downwards when the sliding distance is less than 334.5 Å (corresponding to point A as shown in Fig. 11). The coordinate difference between the slider and substrate is continuously reduced and the dynamic energy is transferred from the slider to substrate. After reaching point A, the velocity direction of the substrate is changed, and the absolute value of the substrate velocity is lower than the slider velocity, so the collision still dominates. And the dynamic energy is also transferred from the slider to the substrate. At point B, the two velocities are the same, and the absolute value of the slider velocity will be lower than the substrate velocity after point B. From then on, the collision is finished and energy is no longer transferred from the slider to substrate.

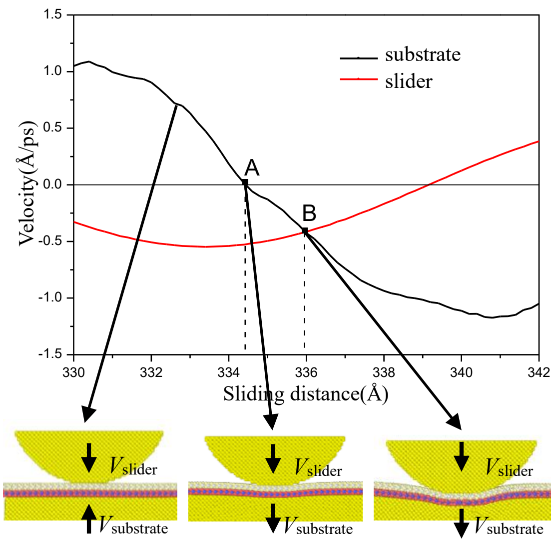


**Fig. 11** The velocities of the slider and substrate at 21.7 GHz

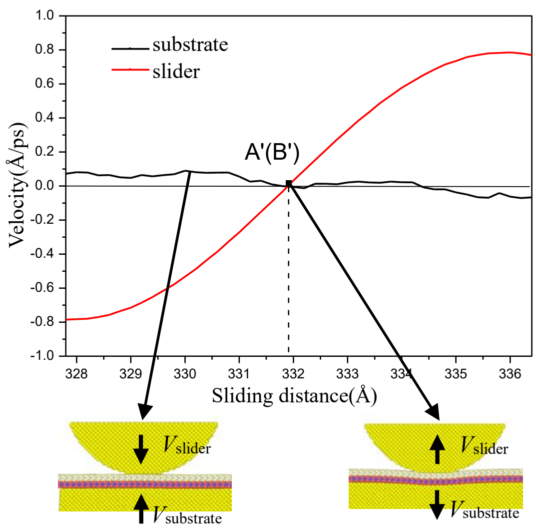


**Fig. 12** The velocities of the slider and substrate at 26.3 GHz

From Fig. 12, when the slider frequency is 26.3 GHz, before point A', the collision process of the slider and substrate is similar to that of 21.7 GHz. From point A’, the velocity direction of the substrate is changed. At the same time, the velocity direction of the slider is changed and the separation occurs. Energy is no longer transferred from the slider to substrate. When the slider frequency is 21.7 GHz, even if the velocity direction of the substrate is changed, the collision continues for a while, which will finally induce a high indentation depth. For the case of 26.3 GHz, when the velocity direction of the substrate is changed, the separation occurs corresponding to point B’, so the collision time between the slider and substrate is short. The time of each collision is 22.4 ps at 21.7 GHz and 16 ps for the case of 26.3 GHz. The longer time the collision, the greater the indentation depth and the higher the average friction force. In the third stage, the collision time becomes shorter and shorter as the frequency increases. Therefore, the average friction forces decrease as the frequency increases. In the fourth stage, when the frequency exceeds 26.3 GHz, the time of each collision is very short and the effect of frequency on the collision friction process is slight. Hence, the average friction forces show slight changes as the frequency increases.

Figure 13 shows atomic snapshots at different frequencies. From the above discussion, when the vibration frequency of the slider is close to the natural frequency of the substrate, the collision friction of the slider and substrate is not severe and there is no dislocation in the substrate at 18.5 GHz in Fig. 13(a). When the vibration frequency is higher than the natural frequency of the substrate, the collision friction is more severe. There are a large number of dislocations in the substrate at 21.7 GHz in Fig. 13(b), and the severe collision friction leads to the plastic deformation of the substrate and the accumulation of atoms on the Au surface. For the case of 26.3 GHz, the collision time between the slider and substrate is short and there is no dislocation in Fig. 13(c).

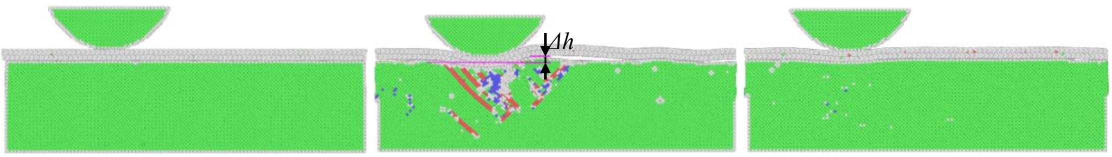


(a) 18.5 GHz (b) 21.7 GHz (c) 26.3 GHz

**Fig. 13** Atomic snapshots at different frequencies

There is severe collision for the case of 21.7GHz in Fig. 13, and phase transition of the $MoS_2$ film may occur. According to the work of Pang et al. (2018a), when the phase transition of $MoS_2$ occurs, the maximum S-Mo bond length could be increased from 2.42 Å to about 2.6 Å, and the minimum S-Mo bond length was also reached 2.55 Å. In view of these, at 21.7 GHz, the atomic snapshot of the $MoS_2$ film under the slider is extracted when the slider reaches its maximum indentation depth, and the S-Mo bond lengths are also calculated. In Fig. 14, S-Mo bonds are colored according to the bond length values. From Fig. 14, even if the indentation is maximum, the structure of the $MoS_2$ is still a regular hexagonal structure of the semiconductor phase and most of the bond lengths are initial bond length values. Only a small part of the S-Mo bond lengths are increased, but none of them exceeds 2.5 Å. As a result, during the collision friction process, the mechanical deformation of the $MoS_2$ film is still in the stage of elastic deformation even under the most severe collision situation, and no structural phase transition occurs in $MoS_2$.

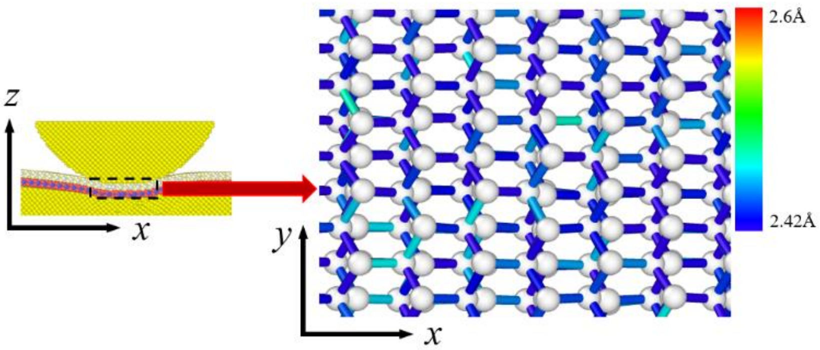


**Fig. 14** The S-Mo bond length distribution map of $MoS_2$ film under the slider

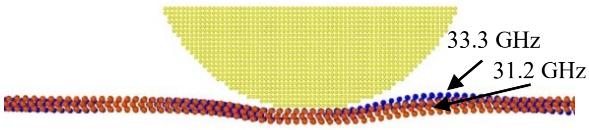


**Fig. 15** Atomic snapshots of the $MoS_2$ film at two frequencies

Figure 15 shows atomic snapshots of the $MoS_2$ film at two frequencies. When the frequency is 33.3 GHz, the $MoS_2$ film in front of the slider is more convex than the case of 31.2 GHz, and the rest of $MoS_2$ film are nearly coincided with the case of 31.2 GHz. At 33.3 GHz, the collision friction leads to a puckering effect in the $MoS_2$ film, and this puckering effect is a main factor affecting frictional properties of two-dimensional layered materials (Cao et al. 2019). This phenomenon also explains why the average friction force at 33.3 GHz is higher than other frequencies in the fourth stage.

### 3.3 The effects of amplitude on collision friction process

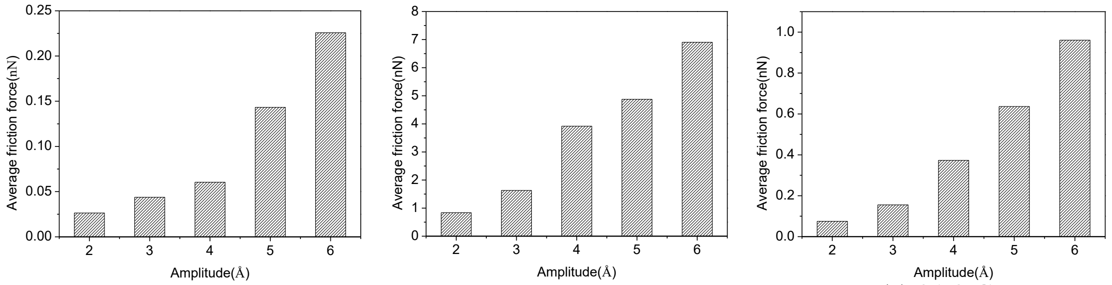


(a) 18.5 GHz (b) 21.7 GHz (c) 31.2 GHz

**Fig. 16** Comparison of average friction forces with different amplitudes at three frequencies

In this work, five vibration amplitudes are selected to study their effects on the collision friction process. Fig. 16 shows the comparison of average friction forces with different amplitudes at three representative frequencies. From Fig. 16, increasing the amplitude at different frequencies will increase the average friction forces. In order to find the reason for the increase in average friction forces, the coordinate difference between the slider and substrate is extracted.

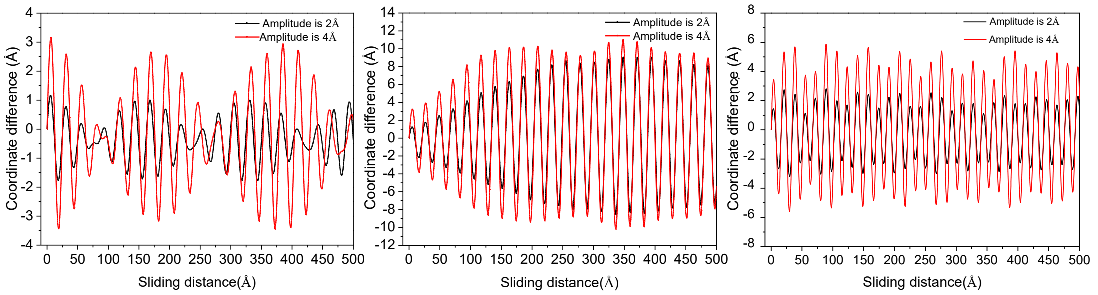


(a) 18.5 GHz (b) 21.7 GHz (c) 31.2 GHz

**Fig. 17** The coordinate difference for different amplitudes at different frequencies

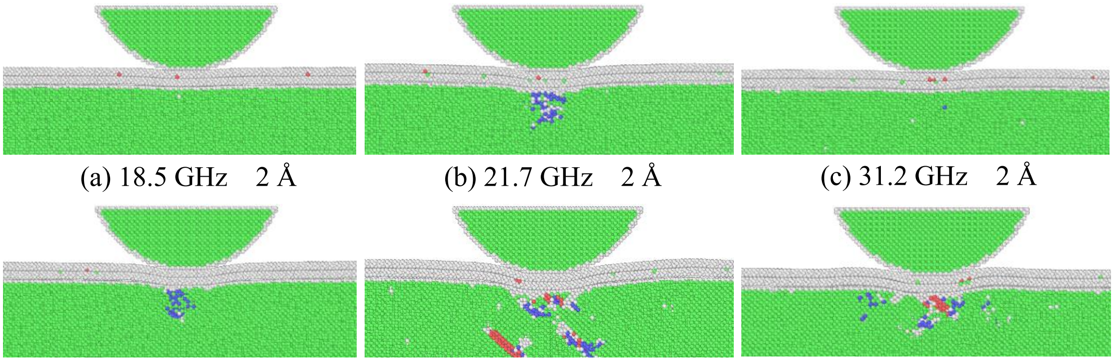

(a) 18.5 GHz 2 Å (b) 21.7 GHz 2 Å (c) 31.2 GHz 2 Å

(d) 18.5 GHz 6 Å (e) 21.7 GHz 6 Å (f) 31.2 GHz 6 Å

**Fig. 18** Atomic snapshots for different amplitudes at different frequencies

Figure 17 shows the coordinate difference between the slider and substrate for different amplitudes at the three frequencies. From Fig. 17, whether at the natural frequency (18.5 GHz) or at 21.7, 31.2 GHz, the higher the amplitude, the greater the fluctuation of the coordinate difference between the slider and substrate. For different frequencies, the absolute values of coordinate difference explain the difference of the average friction forces. In a collision friction process at a specific frequency, increasing the amplitude leads to the increase of the coordinate difference and indentation depth, which eventually leads to an increase in the average friction force. From atomic snapshots at different amplitudes in Fig. 18, increasing the amplitude leads to the increase of dislocation in the Au of the substrate. From Fig. 18(a) and (d) or (c) and (f), increasing the amplitude, the dislocation appears in the Au of the substrate after the amplitude is increased, and the deformation of the Au of the substrate is transformed from the elastic stage to the plastic stage. Besides, from Fig. 18, it is clearly shown that for a same frequency, a high amplitude induces a high indentation depth, and the high indentation depth results in the increase of the friction force.

## 4. Conclusions

In this paper, a collision friction model for a double-layer $MoS_2$ film used in microgravity environment is proposed, and a modified REBO potential is employed to describe interactions among the atoms within the $MoS_2$ film. The effects of collision frequency and amplitude on frictional properties of the $MoS_2$ film are investigated. Finally, the mechanism of the influence of frequency and amplitude on collision friction process is discussed.

Two vibrations are applied on the slider in the *y* and *z* directions, and average friction forces show the dependence of the vibration frequency. For a single vibration in the *y* direction, its influence can be ignored. On the contrary, the influence of the vibration in the *z* direction is significant.

Considering the vibrations in two directions, the variation of average friction forces with frequency can be divided into four stages. In the first stage, the collision friction process is stable and the average friction force fluctuates slightly as the frequency increases. In the second stage, the vibration frequency is greater than the natural frequency of the substrate, and the collision soars as the vibration frequency increases. The more severe collision leads to higher indentation depth and average friction force. In the third stage, the collision weakens as the frequency increases, so the average friction force decreases as the frequency increases. In the fourth stage, the effect of frequency on the collision friction process is slight due to the short duration of each collision, and the average friction force shows little change as the frequency increases.

A puckering phenomenon occurs at a specific frequency and makes the average friction force increased at this frequency.

When increasing the amplitude at different frequencies, the maximum indentation depth is increased, and the average friction force is also increased.

## 5. Acknowledgements

The authors would like to thank the National Natural Science Foundation of China (52075444, 51675429), the Fundamental Research Funds for the Central Universities (31020190503004), and Key Project of National Natural Science Foundation of China (51535009) for their financial support.

## 6. References

Cao, X.A., Gan, X.H., Lang, H.J., Yu, K., Ding, S.Y., Peng, Y.T., Yi, W.M.: Anisotropic nanofriction on $MoS_2$ with different thicknesses. Tribol. Int. **134**, 308-316 (2019)

Cao, X.A., Gan, X.H., Peng, Y.T., Wang, Y.X., Zeng, X.Z., Lang, H.J., Deng, J.N., Zou, K.: An ultra-low frictional interface combining FDTS SAMs with molybdenum disulfide. Nanoscale **10**(1), 378-385 (2018)

Claerbout, V.E.P., Polcar, T., Nicolini, P.: Superlubricity achieved for commensurate sliding: $MoS_2$ frictional anisotropy in silico. Comput. Mater. Sci. **163**, 17-23 (2019)

Colas, G., Saulot, A., Godeau, C., Michel, Y., Berthier, Y.: Decrypting third body flows to solve dry lubrication issue-$MoS_2$ case study under ultrahigh vacuum. Wear **305**(1-2), 192-204 (2013)

Delhommelle, J., Millie, P.: Inadequacy of the Lorentz-Berthelot combining rules for accurate predictions of equilibrium properties by molecular simulation. Mol. Phys. **99**(8), 619-625 (2001)

Fleischauer, P.D.: Effects of crystallite orientation on environmental stability and lubrication properties of sputtered $MoS_2$ thin films. ASLE Trans. **27**(1), 82-88 (1984)

Fleischauer, P.D., Bauer, R.: Chemical and structural effects on the lubrication properties of sputtered $MoS_2$ films. Tribol. Trans. **31**(2), 239-250 (1988)

Fusaro, R.L.: Lubrication and failure mechanisms of molybdenum disulfide films. I - Effect of atmosphere. Technical Paper 1343 NASA (1978)

Fusaro, R.L.: Effect of substrate surface finish on the lubrication and failure mechanisms of molybdenum disulfide films. ASLE Trans. **25**(2), 141-156 (1982)

Gao, X.M., Hu, M., Fu, Y.L., Weng, L.J., Liu, W.M., Sun, J.Y.: $MoS_2$-Au/Au multilayer lubrication film with better resistance to space environment. J. Alloys Compd. **815**, 152483 (2020)

Ghobadi, N.: A comparative study of the mechanical properties of multilayer $MoS_2$ and graphene/$MoS_2$ heterostructure: effects of temperature. number of layers and stacking order. Curr. Appl. Phys. **17**(11), 1483-1493 (2017)

Holinski, R., Gänsheimer, J.: A study of the lubricating mechanism of molybdenum disulfide. Wear **19**(3), 329-342 (1972)

Hou, K.M., Han, M.M., Liu, X.H., Wang, J.Q., He, Y.Z., Yang, S.R.: In situ formation of spherical $MoS_2$ nanoparticles for ultra-low friction. Nanoscale **10**(42), 19979-19986 (2018)

Huang, P., Castellanos-Gomez, A., Guo, D., Xie, G.X., Li, J.: Frictional characteristics of suspended $MoS_2$. J. Phys. Chem. C **122**(47), 26922-26927 (2018)

Huang, P., Guo, D., Xie, G.X., Li, J.: Electromechanical failure of $MoS_2$ nanosheets. Phys. Chem. Chem. Phys. **20**(27), 18374-18379 (2018)

Huang, Y.Z., Liu, L., Yang, J.J., Chen, Y.F.: Nanotribological properties of ALD-made ultrathin $MoS_2$ influenced by film thickness and scanning velocity. Langmuir **35**(10), 3651-3657 (2019)

Irving, B.J., Nicolini, P., Polcar, T.: On the lubricity of transition metal dichalcogenides: an ab initio study. Nanoscale **9**(17), 5597-5607 (2017)

Li, H., Wang, J.H., Gao, S., Chen, Q., Peng, L.M., Liu, K.H., Wei, X.L.: Superlubricity between $MoS_2$ monolayers. Adv. Mater. **29**(27), 1701474 (2017)

Li, M., Shi, J.L., Liu, L.Q., Yu, P., Xi, N., Wang, Y.C.: Experimental study and modeling of atomic-scale friction in zigzag and armchair lattice orientations of $MoS_2$. Sci. Technol. Adv. Mater. **17**(1), 189-199 (2016)

Liang, T., Phillpot, S.R., Sinnott, S.B.: Parametrization of a reactive many-body potential for Mo-S systems. Phys. Rev. B **79**(24), 245110 (2009)

Liang, T., Phillpot, S.R., Sinnott, S.B.: Erratum: Parametrization of a reactive many-body potential for Mo-S systems [Phys. Rev. B **79**(24), 245110 (2009)]. Phys. Rev. B **85**(19), 199903 (2012)

Moore, D.F.: Principles and applications of tribology. Pergamon Press, Oxford (1975)

Nicolini, P., Polcar, T.: A comparison of empirical potentials for sliding simulations of $MoS_2$. Comput. Mater. Sci. **115**, 158-169 (2016)

Onodera, T., Morita, Y., Suzuki, A., Koyama, M., Tsuboi, H., Hatakeyama, N., Endou, A., Takaba, H., Kubo, M., Dassenoy, F., Minfray, C., Joly-Pottuz, L., Martin, J.-M., Miyamoto, A.: A computational chemistry study on friction of h-$MoS_2$. Part I. Mechanism of single sheet lubrication. J. Phys. Chem. B **113**(52), 16526-16536 (2009)

Onodera, T., Morita, Y., Nagumo, R., Miura, R., Suzuki, A., Tsuboi, H., Hatakeyama, N., Endou, A., Takaba, H., Dassenoy, F., Minfray, C., Joly-Pottuz, L., Kubo, M., Martin, J.-M., Miyamoto, A.: A computational chemistry study on friction of h-$MoS_2$. Part II. Friction anisotropy. J. Phys. Chem. B **114**(48), 15832-15838 (2010)

Pang, H.S., Li, M.L., Gao, C.H., Huang, H.L., Zhuo, W.R., Hu, J.Y., Wan, Y.L., Luo, J., Wang, W.D.:

Phase transition of single-layer molybdenum disulfide nanosheets under mechanical loading based on molecular dynamics simulation. Materials **11**(4), 502 (2018)

Pang, H.S., Li, M.L., Gao, C.H., Lai, L.F., Zhou, W.R.: Characterization of frictional properties of single-layer molybdenum-disulfide film based on a coupling of tip radius and tip-sample distance by molecular-dynamics simulations. Nanomaterials **8**(6), 387 (2018)

Park, H., Shin, G.H., Lee, K.J., Choi, S.-Y.: Probing temperature-dependent interlayer coupling in a $MoS_2$/h-BN heterostructure. Nano. Res. **13**(2), 576-582 (2020)

Plimpton, S.: Fast parallel algorithms for short-range molecular dynamics. J. Comp. Phys. **117**(1), 1-19 (1995)

Pope, L.E., Panitz, J.K.G.: The effects of hertzian stress and test atmosphere on the friction coefficients of $MoS_2$ coatings. Surf. Coat. Technol. **36**(1-2), 341-350 (1988)

Quereda, J., Castellanos-Gomez, A., Agrait, N., Rubio-Bollinger, G.: Single-layer $MoS_2$ roughness and sliding friction quenching by interaction with atomically flat substrates. Appl. Phys. Lett. **105**(5), 053111 (2014)

Serpini, E., Rota, A., Valeri, S., Ukraintsev, E., Rezek, B., Polcar, T., Nicolini, P.: Nanoscale frictional properties of ordered and disordered $MoS_2$. Tribol. Int. **136**, 67-74 (2019)

Shi, Y.B., Cai, Z.B., Pu, J.B., Wang, L.P., Xue, Q.J.: Interfacial molecular deformation mechanism for low friction of $MoS_2$ determined using ReaxFF-MD simulation. Ceram. Int. **45**(2), 2258-2265 (2019)

Singer, I.L., Bolster, R.N., Wegand, J., Fayeulle, S., Stupp, B.C.: Hertzian stress contribution to low friction behavior of thin $MoS_2$ coatings. Appl. Phys. Lett. **57**(10), 995-997 (1990)

Spalvins, T.: Deposition of $MoS_2$ films by physical sputtering and their lubrication properties in vacuum. ASLE Trans. **12**(1), 36-43 (1969)

Spalvins, T.: Coatings for wear and lubrication. Thin Solid Films **53**(3), 285-300 (1978)

Stewar, J.A., Spearot, D.E.: Atomistic simulations of nanoindentation on the basal plane of crystalline molybdenum disulfide($MoS_2$). Modelling Simul. Mater. Sci. Eng. **21**(4), 045003 (2013)

Stoyanov, P., Gupta, S., Chromik, R.R., Lince, J.R.: Microtribological performance of Au-$MoS_2$ nanocomposite and Au/$MoS_2$ bilayer coatings. Tribol. Int. **52**, 144-152 (2012)

Stukowski, A.: Visualization and analysis of atomistic simulation data with OVITO – the Open Visualization Tool. Modelling Simul. Mater. Sci. Eng. **18**(1), 015012 (2010)

Takahashi, N., Shiojiri, M., Enomoto, S.: High resolution transmission electron microscope observation of stacking faults of molybdenum disulphide in relation to lubrication. Wear **146**(1), 107-123 (1991)

Tong, R.T., Han, B., Quan, Z.F., Liu, G.: Molecular dynamics simulation of friction and heat properties of nano-texture gold film in space environment. Surf. Coat. Tech. **358**, 775-784 (2019)

Tong, R.T., Liu, G.: Friction property of impact sliding contact under vacuum and microgravity. Microgravity Sci. Tec. **31**(1), 85-94 (2019)

Tong, R.T., Liu, G.: Modelling of unidirectional reciprocating sliding contacts of nanoscale textured surfaces considering the impact effects in microgravity environment. Microgravity Sci. Tec. **32**(2), 155-166 (2020)

Tong, R.T., Liu, G.: Vibration induced reciprocating sliding contacts between nanoscale multi-asperity tips and a textured surface. Microgravity Sci. Tec. **32**(1), 79-88 (2020)

Tong, R.T., Quan, Z.F., Han, B., Liu, G.: Coarse-grained molecular dynamics simulation on friction behaviors of textured ag-coating under vacuum and microgravity environments. Surf. Coat. Tech. **359**, 265-271 (2019)

Tong, R.T., Quan, Z.F., Zhao, Y.D., Han, B., Liu, G.: Influence of nanoscale textured surfaces and subsurface defects on friction behaviors by molecular dynamics simulation. Nanomaterials **9**(11), 1617(1-15) (2019)

Wang, D.F., Yu, H., Tao, L., Xiao, W.D., Fan, P., Zhang, T.T., Liao, M.Z., Guo, W., Shi, D.X., Du, S.X., Zhang, G.Y., Gao, H.J.: Bandgap broadening at grain boundaries in single-layer $MoS_2$. Nano. Res. **11**(11), 6102-6109 (2018)

Wang, J.D., Chen, S., Cui, K., Li, D.G., Chen, D.R.: Approach and coalescence of gold nanoparticles driven by surface thermodynamic fluctuations and atomic interaction forces. ACS Nano **10**, 2893-2902 (2016)

Xing, Y.Q., Wu, Z., Yang, J.J., Wang, X.S., Liu, L.: LIPSS combined with ALD $MoS_2$ nano-coatings for enhancing surface friction and hydrophobic performances. Surf. Coat. Technol. **385**, 125396 (2020)

Yang, J.J., Liu, L.: Nanotribological properties of 2-D $MoS_2$ on different substrates made by atomic layer deposition (ALD). Appl. Surf. Sci. **502**, 144402 (2020)

Zeng, X.Z., Peng, Y.T., Lang, H.J., Yu, K.: Probing the difference in friction performance between graphene and $MoS_2$ by manipulating the silver nanowires. J. Mater. Sci. **54**(1), 540-551 (2019)